

An On-Chip Processor for Chronic Neurological Disorders Assistance Using Negative Affectivity Classification

Abdul Rehman Aslam[✉], Student Member, IEEE, and Muhammad Awais Bin Altaf[✉], Member, IEEE

Abstract—Chronic neurological disorders (CND's) are lifelong diseases and cannot be eradicated, but their severe effects can be alleviated by early preemptive measures. CND's, such as Alzheimer's, Autism Spectrum Disorder (ASD), and Amyotrophic Lateral Sclerosis (ALS), are the chronic ailment of the central nervous system that causes the degradation of emotional and cognitive abilities. Long term continuous monitoring with neuro-feedback of human emotions for patients with CND's is crucial in mitigating its harmful effect. This paper presents hardware efficient and dedicated human emotion classification processor for CND's. Scalp EEG is used for the emotion's classification using the valence and arousal scales. A linear support vector machine classifier is used with power spectral density, logarithmic interhemispheric power spectral ratio, and the interhemispheric power spectral difference of eight EEG channel locations suitable for a wearable non-invasive classification system. A look-up-table based logarithmic division unit (LDU) is to represent the division features in machine learning (ML) applications. The implemented LDU minimizes the cost of integer division by 34% for ML applications. The implemented emotion's classification processor achieved an accuracy of 72.96% and 73.14%, respectively, for the valence and arousal classification on multiple publicly available datasets. The $2 \times 3\text{mm}^2$ processor is fabricated using a $0.18 \mu\text{m}$ 1P6M CMOS process with power and energy utilization of 2.04 mW and $16 \mu\text{J}/\text{classification}$, respectively, for 8-channel operation.

Index Terms—Continuous health monitoring, classification processor, electroencephalogram (EEG), emotion detection, machine learning, neurological disorder, support vector machine.

I. INTRODUCTION

MOTIONS play a vital role in the day to day life activities and decisions. They depict the human mental state and have a huge impact on his physiological, behavioral, and cognitive status. Internal human emotion (IHE) determination has been studied in a lot of applications in the recent past, such as healthcare, military personals psychological assessment,

Manuscript received April 2, 2020; revised June 15, 2020; accepted July 6, 2020. Date of publication July 13, 2020; date of current version August 17, 2020. This work was funded by the Higher Education Commission (HEC), Pakistan under Grant 7978/Punjab/NRPU/R&D/HEC/2017. This article was recommended by Associate Editor Changzhan Gu. (*Corresponding author: Muhammad Awais Bin Altaf*)

The authors are with the Electrical Engineering Department, Lahore University of Management Sciences, Lahore 54792, Pakistan (e-mail: 17060056@lums.edu.pk; awais.altaf@lums.edu.pk).

Color versions of one or more of the figures in this article are available online at <https://ieeexplore.ieee.org>.

Digital Object Identifier 10.1109/TBCAS.2020.3008766

neuro-feedback devices for learning, and memory enhancement [1]. Research shows a lot of chronic neurological disorders (CND's), i.e. Alzheimer [2], Autism Spectrum Disorder (ASD) [3], [4], and Amyotrophic Lateral Sclerosis (ALS) [5], [6] (AAA-CND's) are accompanied with the degradation of emotional and cognitive abilities. Broadly IHE recognition can be classified into detection through 1) physical signals, i.e. facial expression, speech, and posture, or 2) physiological signals, i.e. electroencephalogram (EEG), electrocardiogram (ECG), and temperature. Different machine learning (ML) and deep learning classification techniques based on facial expression have provided quite an accurate prediction of human emotions [7], [8]. Though physical signals are easy to collect, reliability can be challenging especially in AAA-CND's due to the concealment of facial expressions in case of ASD and may not depict the true state of mind [9]. On the other hand, physiological signal tracking does not have issues of reliability or depiction of a true physiological state. But the data acquisition can be a bottleneck. Further on, EEG is the most reliable as it depicts the state of mind [10]. The reflection of the human mental state also enables EEG signals to perform other tasks like motor imagery classification [11], [12], Parkinson's classification [13], [14], or IHE recognition.

Multiple channel EEG signals capture human emotion at finer temporal resolution. A significant amount of research has been done in the area of IHE recognition of EEG signals due to the dependency of our daily activities on emotions and technological advancements in the area of miniaturized EEG acquisition systems [15]. Negative affectivity (NAF) refers to a personality attribute to continuously encounter negative emotions. People affected by NAF experience a higher frequency of negative emotions irrespective of the situation [16]. It reflects the bias of the human cognition towards the negative esteem of emotions [17]. There is a significant amount of research to predict the NAF of a person using their EEG signals [18]. But, despite the significant efforts done in the past two decades, still, no reliable wearable EEG-NAF recognition system is available. Moreover, even the focus in research is more towards a software-based solution for emotion detection, which has real-time limitations due to large decision latency. To ensure maximum benefit from the emotion detection, it necessitates a wearable device like hearing aids, smartwatch, or a headband to capture real-time emotion and provide neuro-feedback for early and meaningful intervention.

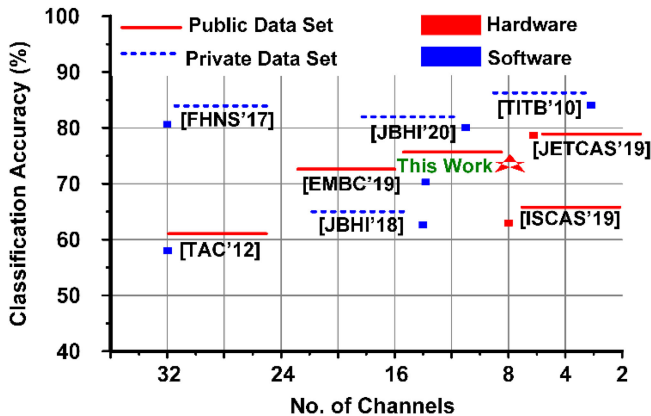


Fig. 1. Trend of EEG NAF classification systems.

Fig. 1 shows the trend of EEG-NAF systems in the past two decades and asserts that recent and past works have focused primarily on software implementations [19]–[32]. Most of the works have utilized ≥ 14 EEG channels for emotion detection with significantly complex feature extraction (FE) and classification engine [24]–[30]. An area- and energy-efficient System on Chip (SoC) with integrated FE, patient-specific (PS) emotion classification, and EEG recording enabling a patch form-factor device for continuous emotion detection [32]–[34] is required for the problem mentioned.

The problems with available emotion classification solutions include:

- 1) *Software implementation with a local dataset.* The algorithms proposed in [20], [23], and [28] reported a good classification accuracy but lack hardware implementation and even the reported high classification results are based on the private (local) datasets. The results can't be validated, hence not suited for real-time implementation.
- 2) *Based on a lot of channels.* Ref [22], [27], [29], [30] though implemented in software with reasonable accuracy ranging from 62% to 95% using public emotion datasets, but utilize a large number (>8) of channels for the evaluation. The utilization of a lot number of channels (>8) is a bottleneck in the real-time realization due to patient-comfort and battery constraints.
- 3) *Software implementation with complex FE and Classification.* The emotion detection algorithm in [21]–[23] though implemented in software with public emotion datasets, but the FE and classification approaches are fairly complex, which will lead to expensive hardware realization with the long battery requirement.
- 4) *Hardware implementations:* Ref [8], [35] have provided the hardware implementations for emotion recognition using facial expressions. The facial expressions can be intentionally regulated unlike EEG signals [36], therefore, can be deceptive for AAA-CND, whereas, the EEG signals provide a realistic emotion representation. The facial expression definitely will be the ideal scenario based on the certain application requirement, but for a wearable system with the minimal latency requirement, the EEG system seems a preferable choice.

Ref [37] implemented emotions recognition SoC using EEG signals while achieving good classification accuracy of 76.67% on benchmark dataset [21]. Though the implemented system utilizes only 6-channel with an area utilization of 3.35mm^2 but consumes high power (76.6mW), which will not suit the target application of our system. Moreover, they have validated only on a single dataset which limits its robustness.

This work focuses on emotion detection with an explicit target on CND rehabilitation, to enhance the social interaction of patients affected by AAA-CND's. The common scenario regarding the AAA-CND is their lacking emotional expressions and social limitations. The main technical challenges and contributions of this work are:

To overcome the limitations of the available software approaches [19]–[30] and design a hardware-efficient emotion detection algorithm [38] to be realized on-chip.

- 1) An efficient set of FE engine is selected to enhance the accuracy comparable to the state-of-the-art software solutions.
- 2) Proposed and implemented a logarithmic interhemispheric power spectral ratio (LIHPR) for efficient on-chip implementation.
- 3) Proposed and implemented a logarithmic division unit (LDU) to reduce the hardware cost by 34%.

Utilize reduced number of EEG channels (8) to ensure patient comfort and wearable system yet not compromising the classification accuracy.

The proposed system is the first on-chip implementation of the EEG based emotion detection for AAA-CND's using a 180nm CMOS process with:

- 1) Validation on multiple benchmark EEG datasets for real-time emotion classification.
- 2) The measured latency and power consumption of <1 min and 2.04 mW, respectively.

The rest of this paper is organized as follows. Section II describes the roles of emotions for different CND's. Section III and Section IV describe the emotions classification algorithm and hardware implementation, respectively. Section V provides performance comparison and section VI concludes the usefulness of this work.

II. SOCIAL INTERACTION AND EMOTIONS

The major remedy of AAA-CND's is an early and meaningful intervention to enhance their social, learning, and cognitive abilities. ASD directly affects the cognitive level of the patients as a certain level of cognition is necessary to interpret the emotions correctly [39]. Most of the ASD patients are unable to identify their emotions (suffering from Alexithymia [40]). One of the major challenges in the rehabilitation of ASD patients is to train them to express their emotions properly [41]. Alzheimer's affects a person's memory, not the emotions but they also fail to express their emotions. Therefore, emotional processes in the early stages of Alzheimer's lead to better predictors for developing the disease and can help in reducing the severity of it. Further on, ALS considered for a long time a motor neuron disease also deficits in emotional and cognitive processing. In

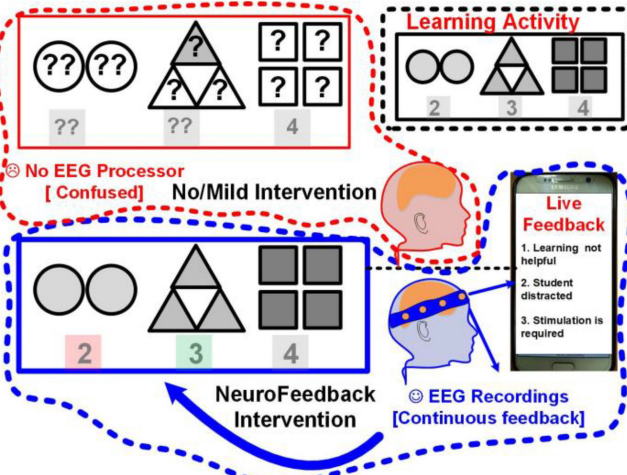


Fig. 2. Proposed AAA-CND's rehabilitation solution illustration.

all the three AAA-CND's, the person is not expressive of his/her emotions and that can lead to a handicapped life.

Fig. 2 depicts the broad idea of the implemented system that supports a learning deficit child during specific learning activities. The top marked as red is a teaching method without any intervention and not tuned to one's learning abilities and therefore not effective for him. Since the learning deficit subject is affected by the limited social syndrome and unable to express his NAF, therefore, fails to get any benefit from the learning activity. The bottom part (blue dotted) shows the proposed effective intervention system which will extract the EEG data, process the information, and assist the caregiver in molding the learning activity tuned to the specific subject needs. The presented figure exemplifies the problem in social interaction and how the proposed device with real-time human emotion/behavior detection can play a vital role in coping with social interaction issues, especially in AAA-CND's.

III. EEG EMOTION'S CLASSIFICATION

Emotion classification using EEG signals is a very challenging problem in-comparison to other EEG classification tasks, i.e., epilepsy detection [38], and motor imagery tasks [11], [12], [42] or depth of anesthesia detection [43]. It lacks specific event-related potentials and medically verified annotation system for the labels. Labels are based on the user's self-experiences and ratings, which makes their classification challenging as they can also be deceitful [44].

Emotions are either classified into a discrete set of emotions [44] or a bi-dimensional scale proposed by Russel [45] in the circumplex model of the effect. They utilized valence and arousal scale to classify 28 different emotions. Valence expresses the scale of positivity or negativity of emotion and arousal represents the strength of that positivity or negativity. For the emotion classification using EEG signals, different EEG datasets for emotion classification exist. DEAP [21] and SEED [22] are the most extensively evaluated emotion classification datasets. DEAP [21] is considered as a benchmark among the researchers

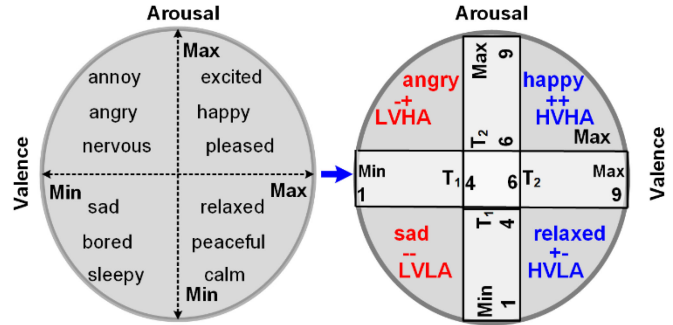


Fig. 3. Valence and arousal scale of emotions for DEAP dataset.

because of the large number of subjects and challenging complexity to achieve high classification results. Some people have utilized the self-recorded private datasets and reported quite high classification results [46]. But those results are not comparable with benchmark and publicly available datasets as their results can be highly overfitted due to the limited number of subjects. In the presented work, both DEAP and SEED are utilized for the analysis and design of the proposed emotion classification processor to ensure the robustness of the processor against any unknown EEG data.

A. Emotions EEG Datasets

The DEAP dataset was recorded and made publicly available by the Queen Mary University of London. It contains the physiological signals of thirty-two participants during forty different emotional states. The emotional states were labelled using valence, arousal, dominance, liking, and familiarity. A scale of 1 (minimum) to 9 (maximum) was used for the labels except for familiarity. The familiarity was scaled between 1 (minimum) to 5 (maximum). The sampling frequency of the dataset was 512 Hz [21].

The SEED dataset was recorded by Jiao Tong University, China (Brain-like computing and Machine-Intelligence (BCMI) lab). [22]. It contains the EEG signals of fifteen subjects for fifteen emotions in three different sessions. The emotions were labelled as positive, neutral, and negative on the valence scale. Sixty-two electrodes were used to record the EEG signals at a sampling frequency of 1000 Hz [47], [48].

B. Emotions' Classification Algorithm

Different emotions mapped on the valence-arousal scale are shown in Fig. 3. The familiarity and liking labels are not used for the emotion classification as they are biased towards the subject and hence not suitable for non-patient specific (NPS) emotion's classification. In the NPS approach, the same learned parameters are used across all patients, i.e. there is no need to learn individual-specific patterns whereas PS approach necessitates separate learning parameters to be uploaded for the classification of each patient.

The valence and arousal scales are distributed into negative, neutral, and positive valence/arousal between their minimum (Min) and maximum (Max) values. T_1 and T_2 are used to define

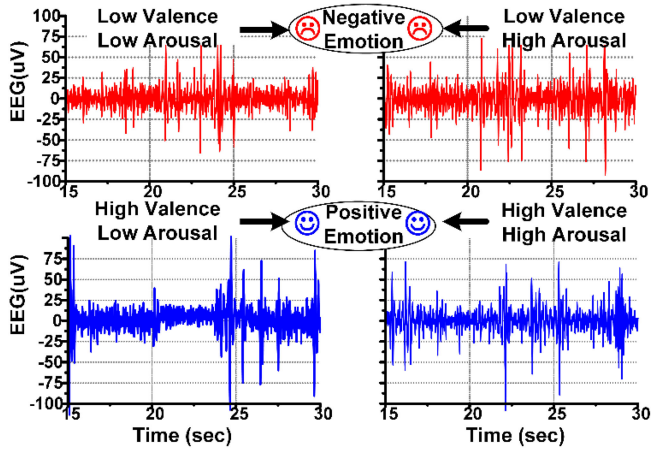


Fig. 4. Temporal EEG plot for LVLA, LVHA, HVLA and HVHA emotions.

the thresholds for neutral valence and arousal. The Min, Max, T_1 , and T_2 for this work are 1, 4, 6, and 9, respectively, to categorize positive and negative valence and arousal.

We classified a set of four emotions, including sad, angry, relaxed and happy corresponding to low valence-low arousal (LVLA), low valence-high arousal (LVHA), high valence-low arousal (HVLA) and high valence-high arousal (HVHA), respectively, using a binary classification of valence and arousal. Emotions are classified using Russel's valence and arousal scale [45].

We classified a set of four emotions, including sad, angry, relaxed and happy corresponding to low valence-low arousal (LVLA), low valence-high arousal (LVHA), high valence-low arousal (HVLA) and high valence-high arousal (HVHA) respectively, using a binary classification of valence and arousal. Emotions are classified using Russel's valence and arousal scale [45].

Fig. 4 shows the temporal EEG plot for the F7 channel of a male participant (subject # 27 in the DEAP dataset) of LVLA, LVHA, HVLA, and HVHA. The detailed temporal and spectral analysis of different frequency bands for low/high valence/arousal did not provide any evident visual markers to distinguish among LVLA, LVHA, HVLA, and HVHA corresponding to sad, angry, happy, and relaxed emotions, respectively. The emotion's classification becomes a daunting challenge due to the unavailability of visible markers to distinguish them. Therefore, the EEG emotion classification requires ML algorithms to extract the deeply hidden information required to identify the correct emotion.

C. Hardware Realizable Emotions' Classification

The previous works in EEG based emotion classification are on an algorithmic level and have much flexibility in terms of the number of channels, large complicated feature vector (FV), and classifier (CLS) complexity. The maximum number of EEG channels (14-64), complex FE engine, and classification algorithms are utilized to achieve the best possible ML classification results [19], [20], [18]–[36]. Moreover, efficient neuromorphic

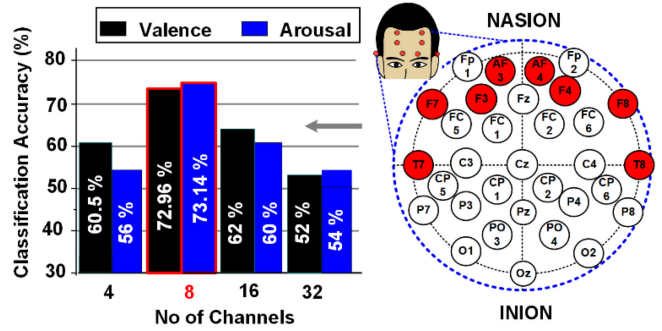


Fig. 5. Scalp locations of selected electrodes and their classification accuracies.

architectures for real-time learning systems with a focus on EEG [11], [49], and generic applications [52], [53] are implemented. We focused on the following factors while optimizing our system for efficient hardware implementation.

1) Channel Selection: To integrate the proposed processor on-sensor, a limited number of channels (≤ 8) are desired to achieve efficient hardware implementation [38]. On-sensor integration is targeted to provide a wearable system for real-time emotion classification. However, reducing the number of channels can have a negative effect on classification accuracy. Therefore, it is important to analyze the number and location of the channel and its effect on classification accuracy. The channel selection process involves the selection of appropriate channels that would provide good classification results [18]. It also involves the selection of channel locations that would cause minimum discomfort to the patients. The complete set of 32 EEG channels was initially investigated. Multiple experiments were conducted by selecting multiple channel combinations to optimize both no. of channels and their location for a hardware-efficient classification processor.

An 8-channel pool (F3, F4, F7, F8, AF3, AF4, T7, and T8) of EEG electrodes were chosen for the implemented emotions classification processor. The selected set of electrodes was chosen on account of the best classification results and the electrode placements based on the international 10-20 system. These electrodes are located on the frontal and temporal locations.

The temporal and forehead locations are more feasible for long-term continuous monitoring of EEG data and will be less frustrating for AAA-CND affectees. Moreover, the selected frontal and temporal EEG channel locations are linked to human emotions and behaviors, hence recommended for emotion classification [18]. Therefore, the exclusion of any of them resulted in accuracy reduction and leads to an under-fitting problem. Furthermore, the accuracy starts to dip again for > 8 channels. This dip is most likely because of the over-fitting problem due to redundant information and complex feature vector formation which decreases the validation accuracy. The classification results of the selected combination with the placement on a human forehead in addition to the classification results on other channel combinations are shown in Fig. 5.

2) Feature Vector Selection: The complexity of the FE algorithm directly affects the overall area and the energy of the classification processor. Therefore, it is critical to analyze the

TABLE I
FEATURES AND HARDWARE RESOURCES

Feature	Classification Accuracy (VAL/ARR)	Area* (# of Gates)	Power* (μW)
Mean (μ)	55.0% / 50.2%	0.49K	10
Root Mean Square (RMS)	50.0% / 56.2%	1.05K	30.3
Standard Deviation (σ)	60.1% / 57.5%	1.12K	22.2
Variance (σ^2)	45.0% / 52.5%	2.68K	50.04
Common Spatial Pattern (CSP)	75.3% / 74.7%	11.75K	185
Hjorth Parameters	68.3% / 54.5%	8.06K	150.1
Entropy	68.0% / 70.4%	4.25K	78.3
PSD, AIHPD, IHPR	71.3% / 72.5%	1.71K	34.2
PSD, AIHPD, LIHPR	72.96% / 73.14%	1.37K	20.1

*Post Synthesis.

hardware implementation cost of the FV in addition to the classification results.

An FV containing the complete EEG signal for the selected channels was used. It contained 60K 10b integer numbers. Different ML classifiers (ML-CLS) were applied for valence and arousal classification. The best-case classification accuracies of >70% were obtained for valence and arousal, respectively. But that would be unrealizable from a hardware perspective due to huge on-chip memory (>1MB) requirement for floating-point (FP) weights to be uploaded on-chip for classification. Moreover, we investigated each EEG channel independently by replicating the label for each channel. It formed an FV of 7.5K x 10b integer numbers. This FV provided quite high best-case classification results (>90%). Despite the high accuracy, we did not proceed with its hardware implementation due to high biases towards certain subjects. The variation in classification accuracy among subjects was huge (>40%) and will fail as a generic approach. It would require ~250 KB of on-chip memory for the FP weights of classification parameters.

To assess the hardware cost for the extraction of various features (temporal and spectral), we used the power consumption, area utilization, and the classification accuracy, to estimate the most optimal choice for our work.

Common spatial patterns (CSP) and the set of power spectral density (PSD), absolute interhemispheric power spectral difference (AIHPD), and interhemispheric power spectral ratio (IHPR) provided the best classification results for the emotion's classification, as shown in Table I.

The hardware implementation of the CSP was not feasible considering strict hardware budget constraints due to the involvement of covariance matrices. The covariance matrix implementation required a huge memory (>5 MB), therefore, we avoided to implement CSP for our on-chip emotion classification processor despite good classification results.

The beta band (12 Hz to 30 Hz) is extensively used in prior works and related to NAF classification [54]. PSD is a prominent feature used to extract meaningful information from the EEG frequency bands [18]. The differences and ratio of the asymmetric electrodes generate supportive features for emotions prediction [23]. Therefore, an FV in (1) comprising of PSD, AIHPD, and IHPR in the beta band was used for our emotion classification processor. The PSD provides the power spectral information and the AIHPD and IHPR provide the differences and ratio of the PSD of the selected right and left hemisphere channels. The selected FV provided us with good classification accuracies for emotion classification and was chosen as an optimal choice. Table I contains the area and power information based on selected synthesized FV's, along with classification accuracies.

$$FV = \{PSD, AIHPD, IHPR\} \quad (1)$$

The PSD is the power of the signal and is calculated by passing the EEG signal through a bandpass filter (BPF) and accumulating the filtered signal for the selected EEG-channels as defined in (2).

$$PSD = \sum_{i=0}^N (|Xn|) \quad (2)$$

PSD_{Left} and PSD_{Right} are the PSD of selected right and left hemisphere channels, respectively, as mentioned in (3) and (4), respectively.

$$PSD_{LEFT} = PSD \{T7, F7, F3, AF3\} \quad (3)$$

$$PSD_{RIGHT} = PSD \{T8, F8, F4, AF4\} \quad (4)$$

AIHPD is the absolute spectral energy difference and IHPR is the power spectral energy ratio between the right and left hemisphere EEG channels, respectively, as defined in (5) and (6), respectively.

$$AIHPD = |PSD_{(Left)} - PSD_{(Right)}| \quad (5)$$

$$IHPR = PSD_{LEFT}/PSD_{RIGHT} \quad (6)$$

To realize (6) on-chip, a divider is required, which will increase the overall area and energy requirement for the processor. Therefore, (6) is rewritten as (7) and (8), by benefitting from the ratio to difference conversion property of logarithms.

$$IHPR = 2 \left[\log_2 \left(\frac{PSD_{LEFT}}{PSD_{RIGHT}} \right) \right] \quad (7)$$

$$IHPR = 2[\hat{\log}_2(PSD_{LEFT}) - \hat{\log}_2(PSD_{RIGHT})] \quad (8)$$

This ratio to difference property of logarithms is beneficial for the hardware implementation of logarithmic ratios of two numbers using a lookup table (LUT) implementation. Eq. (8) requires only the square root of the memory compared to (7). Since (8) requires only storage of \log_2 values of PSD_{LEFT} and PSD_{RIGHT} , whereas for (7) realization on-chip requires all possible values of $PSD_{LEFT} \div PSD_{RIGHT}$ to be stored. Moreover, to get rid of antilog (2^x) mentioned in (8), a modified logarithmic IHPR (LIHPR) defined in (9) is proposed and

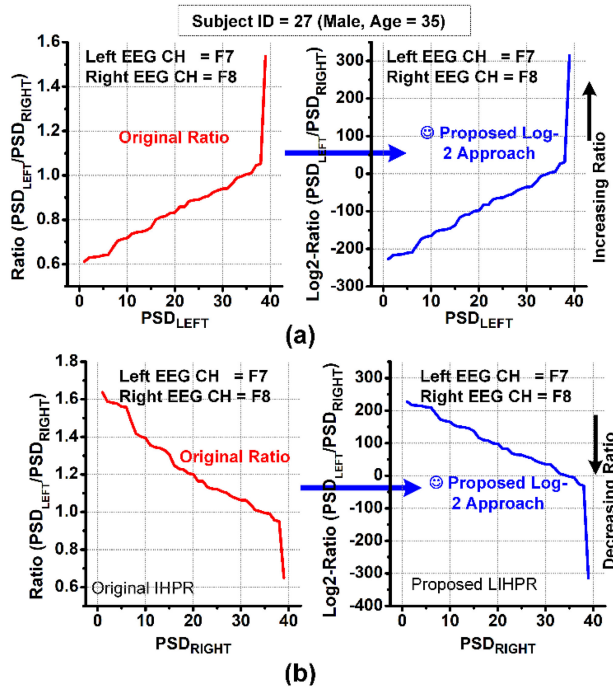


Fig. 6. Comparison of IHPR and LIHPR for (a) increasing and (b) decreasing trend.

implemented. It includes the IHPR information embedded in LIHPR and can be retrieved after the antilog (2^x) operation. But the modified LIHPR (9) does not hamper the classification accuracy compared to IHPR (8) since LIHPR has the information of IHPR and the ML-CLS will train accordingly.

$$LIHPR = \log_2(PSD_{LEFT}) - \log_2(PSD_{RIGHT}) \quad (9)$$

To ensure a similar trend in (8) and (9), IHPR and LIHPR of a subject are shown in Fig. 6(a) and Fig. 6(b), respectively. Fig. 6(a) shows a constant PSD_{RIGHT} and a variable PSD_{LEFT} (ranging from min (index 1) to max (index 40)) for both IHPR and LIHPR, whereas Fig. 6(b) shows vice-versa. Both show that the LIHPR follows a similar pattern as IHPR, and it also provided similar classification results. The proposed LIHPR architecture reduces the gate counts, and power consumption by 4.7X, and 1.5X, respectively, compared with the IHPR.

3) *Feature Normalization:* Feature normalization (FN) is an important preprocessing step in the ML classification where all the features are normalized to a uniform range. The normalized FV ensures the equal role of each feature in the classification. We used the z-score FN that normalizes the FV to a zero mean and unit variance. The FV (F_{1-16}) is normalized to FN_{1-16} as in (10).

$$FN_{1-16} = (F_{1-16} - \mu_{F_{1-16}}) \times \frac{1}{\sigma_{F_{1-16}}} \quad (10)$$

μ_{1-16} and $1/\sigma_{1-16}$ are the mean and inverse standard deviation of F_{1-16} , respectively. The classification results of pre-and-post FN for emotion classification are shown in Fig. 7. It depicts that the FN significantly improved the overall classification performance of the proposed processor.

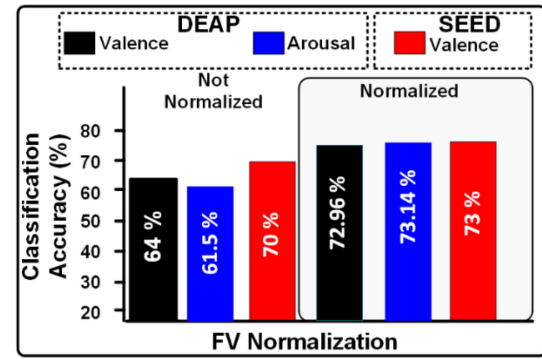


Fig. 7. Classification with and without feature normalization.

TABLE II
FEATURE EXTRACTION ALGORITHM

Algorithm: Feature Extraction Algorithm.
Input: EEG, ch-sel, μ_F , $1/\sigma_F$
Output: FN
Initial: EEG-BPF=0 , PSD=0, AIHPD=0, LIHPR=0, FV=0
 1. if (ch-sel[clk] == ch-sel[clk-1]) // indicates change in channel selection
 2. begin
 3. for ch-sel:=1 to ch-sel:=8 // repeat for each channel
 4. begin
 5. for epochs:=1 to epochs:=5760
 6. // 128 Hz x 45 sec =5760 samples
 7. begin
 8. EEG-BPF[i]:=BPF(EEG[i]) // calculates PSD
 9. end
 10. PSD[ch-sel]:=EEG-BPF // store the PSD
 11. end
 12. else
 13. EEG-BPF=0 // reset PSD calculation for each channel
 14. for k:=1 to k:=4 // calculate four AIHPD's and LIHPR's
 15. begin
 16. AIHPD[k]:=|PSD[2k-1] - PSD[2k]|
 17. // AIHPD[1,2,3,4]=abs(PSD[1,3,5,7]-PSD[2,4,6,8])
 18. LIHPR[k]=log2(PSD[2k-1])-log2(PSD[2k])
 19. // LIHPR[1,2,3,4]=log2(PSD[1,3,5,7])-log2(PSD[2,4,6,8])
 20. end
 21. FV[1:16]=(PSD[1:8],AIHPD[1:4],LIHPR[1:4])
 22. // calculate FV from PSD, AIHPD and LIHPR
 23. FN[1:16]= FV[1:16]- μ_F [1:16] x inverse (σ_F [1:16])
 24. // normalize FV using normalization parameters
 25. return FN

4) *Feature Extraction Algorithm:* The FE algorithm to calculate the normalized feature vector (FN) from the incoming EEG signals of the selected channels is presented in Table II. The incoming EEG signal (EEG) and corresponding channel number (ch-sel) are provided to the FE algorithm to calculate the FN to be forwarded to the classifier. The EEG signals of the

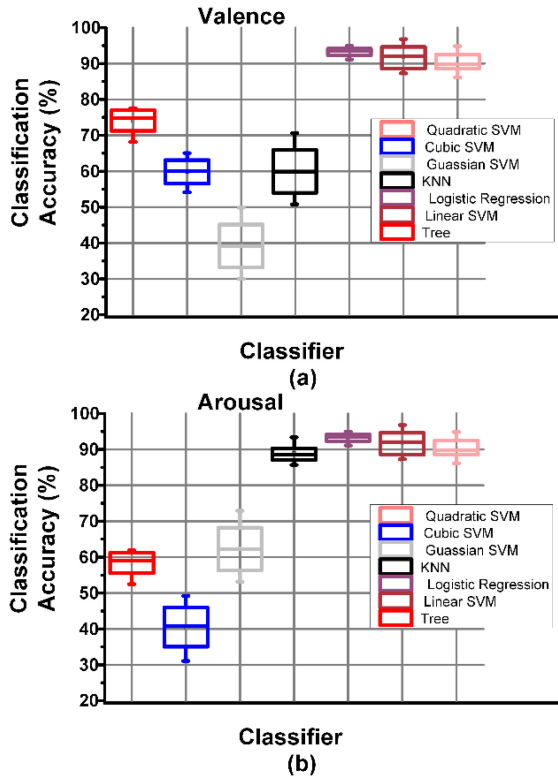


Fig. 8. Classification results for (a) valence and (b) arousal with different CLS based on DEAP dataset.

selected eight left and right hemisphere channels are forwarded in an alternative and sequential manner. The channel is identified by ch-sel to calculate and store the relevant features.

The PSD of each channel is calculated after passing the 5760 epochs of each EEG channel down sampled at 128 Hz corresponding to 45 seconds duration. Each sample is passed from the BPF which is accumulated to calculate the PSD of each channel. The four absolute interhemispheric differences (AIHPR [1:4]) and logarithmic ratios (LIHPR [1:4]) are calculated using the PSD of eight channels (PSD [1:8]). The FV [1:16] is calculated by combining PSD [1:8], AIHPR [1:4] and LIHPR [1:4]. The FN is obtained by subtraction and multiplication of the FV with a mean (μ F) and inverse standard deviation ($1/\sigma$ F) parameters for each channel. The ML classifier utilizes the FN for valence and arousal labels calculation.

5) *Classifier Selection:* An ML classification algorithm is used to calculate the label using the FV. The CLS selection is a composite procedure and depends on a trade-off between classification results and the hardware complexity. The selected FV was classified with different classifiers, including linear regression (LR), decision tree (DT), support vector machine (SVM) with linear and radial basis kernel functions (RBF), k nearest neighbor (KNN) and naïve Bayes (NB). The box chart in Fig. 8 shows the best subject classification results with each CLS.

LR is popularly used for binary classification and it requires a sigmoid activation function. Moreover, LR was not able to classify all the subjects. DT is widely used for binary classification problems like cognitive impairment, agriculture crop

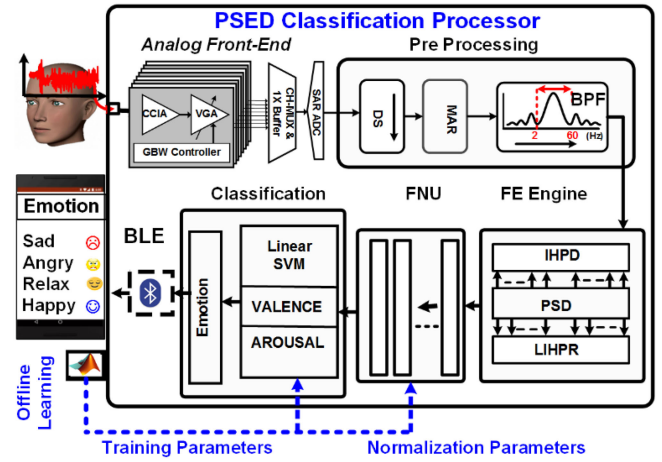


Fig. 9. PSED emotion's classification processor architecture.

classification, and sentiment analysis [55]. It was unable to provide good classification accuracies ($\geq 60\%$) for both valence and arousal classification and not suitable for hardware implementation due to subject dependent variable-length trees. SVM classifier finds a hyperplane in a k-dimensional space to separate the two classes for binary classification. It consumes lesser computational power with good classification accuracy ($\geq 60\%$) [56]. KNN requires more time to predict the output class as it requires several distances to be computed [57]. It did not provide good classification results ($\geq 60\%$) with a uniform distance metric.

NB is a probabilistic model of classification. It is mostly used for spam filtering, recommendation systems, and text classification. The hardware implementation of the NB requires an exponential function and FP divider implementation with high precision. We selected the linear SVM (LSVM) classifier for the hardware implementation as it provided good classification accuracies for the binary classification. It also required a 0.19 KB of on-chip memory compared to 31 KB for the classification parameter storage compared to the SVM-RBF.

IV. HARDWARE IMPLEMENTATION

The implemented SoC consists of an Analog front end (AFE), a successive approximation analog-to-digital converter (SAR-ADC), the pre-processing unit (PU), FE engine, and classification unit. The AFE is composed of 8-channels, where each channel utilizes a low-noise capacitive coupled instrumentation amplifier (CCIA) and programmable gain amplifier (PGA), similar to that of [38], [58]. The implemented CCIA deals with flicker noise, electrode dc offset, 50/60 Hz of interference, and large electrode impedance for wearable EEG environment by incorporating chopping, dc servo loop (DSL), high common-mode rejection ratio and positive feedback loop, respectively [38]. A maximum gain of 80dB is provided to amplify an EEG signal up to $10 \mu V$. The amplified EEG data is digitized by utilizing a 10b SAR ADC, multiplexed among all channels. The digitized data is fed to the digital backend processor designed for EEG-NAF classification. The overall architecture of the proposed PSED

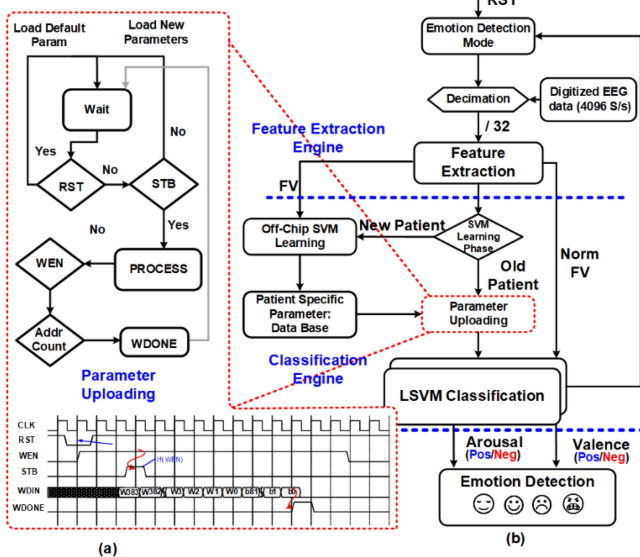


Fig. 10. (a) Parameter uploading for the EEG-NAF classification processor
(b) The state diagram for the EEG-NAF classification processor.

emotion's classification processor is shown in Fig. 9. The classification results are transmitted and displayed on the mobile phone using a low energy Bluetooth (BLE) communication module.

Fig. 10 shows the state diagram of the proposed PSED emotion's classification processor. The EEG data is preprocessed, features are extracted, PS or NPS parameters are uploaded, valence, and arousal classification are performed, and emotion is determined.

The parameter uploading is performed using write-enable (WE), strobe (STB), write data in (WDIN), write data out (WDOUT), and write done (WDONE) inputs and outputs. The WEN and STB initiate the parameters uploading serially through WDIN. The WDONE indicates the completion of the parameters uploading.

Fig. 10(a) shows the parameter uploading process which starts when the STB and WEN inputs are asserted after reset. The parameters are forwarded serially through WDIN, and WDONE indicates the completion of the parameter uploading process. Fig. 10(b) illustrates the complete EEG-NAF classification process by a state diagram. The digitized and decimated EEG data is forwarded to the FEE to calculate the FV. The classification parameters are acquired from the parameter database and uploaded serially as explained previously. The FV and the classification parameters are forwarded to the LSVM classification unit (CFU) for valence and arousal classification. The valence and arousal classes are then used to determine the emotion as LVLA, LVHA, HVLA, or HVHA.

A. Pre-Processing of EEG Data

To deal with an enormous amount of EEG data for storage and later visualization by neurologist, efficient data compression techniques have been adopted in the literature [49], for applications like sleep [50], [51] and seizure [38], where long term

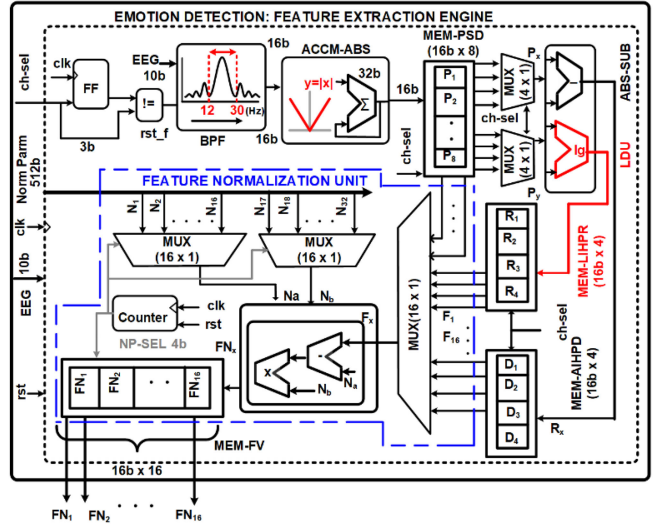


Fig. 11. Feature extraction engine and feature normalization unit.

recording is essential. In the implemented work the incoming raw EEG data sampled at 4096S/s is down-sampled to 128 Hz using a programmable down-sampling unit (DS) to reduce the hardware processing cost. Moreover, to minimize the artifacts (eye blinking, chewing, etc.) and noise, a mean average referenced (MAR) filter and a BPF with a range of 2-60 Hz are utilized, respectively.

B. Feature Extraction Engine

The FE engine is used to calculate the FV. The hardware architecture of the FE engine, including the feature normalization unit (FNU), is shown in Fig. 11. The FV consists of 16×16 b FP numbers ($F_1 - F_{16}$) including the PSD ($P_1 - P_8$), AIHPD ($D_1 - D_4$), and LIHPR ($R_1 - R_4$). The PSD (2) is calculated in the beta band (12-30 Hz). A 3b channel selection input (ch-sel) is used for EEG channel indication. A comparator followed by a 3b flip flop indicates the change in ch-sel to reset the BPF. The incoming EEG data of the eight channels are forwarded to the FE engine in a systolic fashion. This utilized 8X times lower area and input pins than parallel implementation. The BPF is implemented using a finite impulse response (FIR) filter of the 50th order utilizing the least square method to minimize the number of filter coefficients.

The passband and stopband frequencies of the filter are 0db and -43 db, respectively, to maximize the SNR. PSD is calculated by accumulating the absolute values of BPF using a 32b integer accumulator and absolute unit (ACCM-ABS). The output of the ACCM-ABS is quantized to 16b and stored in a memory block (MEM-PSD) of 8×16 b as $P_1 - P_8$. The ch-sel provides the address input for the MEM-PSD.

AIHPD and LIHPR are calculated by absolute subtraction (ABS-SUB) and logarithmic division units (LDU), respectively. Two 4 x 1 multiplexers are used to select one right-left PSD pair ($P_{1,3,5,7}$ and $P_{2,4,6,8}$, respectively, as inputs of the ABS-SUB and LDU using ch-sel. AIHPD is calculated using 16b FP subtractor and substituting the sign bit with zero.

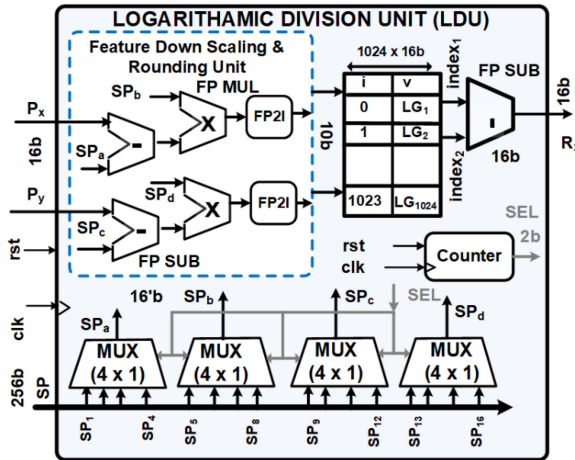


Fig. 12. Block-level diagram of logarithmic division unit.

AIHPD is stored in a memory block (MEM-AIHPD) of $4 \times 16b$ as $D_1\text{-}D_4$ using ch-sel [1:0] as address input.

The hardware architecture of the LDU is shown in Fig. 12. The logarithmic function used in LIHPR is usually implemented by using a LUT, piecewise approximation, or CORDIC algorithm [59]–[61]. The LUT based implementation of the LIHPR of two 16b FPPSD's requires 1 MB of memory. Four 4×1 multiplexers are used to select the downscaling and rounding parameters ($SP_A\text{-}SP_D$) of the right-left PSD pair (P_X and P_Y) that are fed by the FE engine. A 2b selection input SEL provided by a counter is used to select $SP_A\text{-}SP_D$ from $SP_1\text{-}SP_{16}$. $SP_1\text{-}SP_{16}$ is obtained from the 256b down-scaling and rounding parameters input (SP) derived from the parameter register. The downscaled and rounded PSD's of the right-left PSD pair P_X and P_Y are forwarded to the LIHPR as index₁ and index₂, respectively. The $1024 \times 16b$ LUT calculates the LIHPR of index₁ and index₂ using a 16b FP subtractor (FP-SUB) as in (8). The LIHPR of P_X and P_Y are forwarded to the FE engine as R_X . The FE engine stores the R_X into a memory register of $4 \times 16b$ using ch-sel as the address input. The FV including the PSD, AIHPD, and LIHPR stored as $P_1\text{-}P_8$, $D_1\text{-}D_4$, and $R_1\text{-}R_4$, respectively, are forwarded to the FNU as $F_1\text{-}F_{16}$.

A feature down-scaling and rounding unit is used to scale and round off, respectively, the PSD's from a broader range to a narrower range. The PSD's can be downscaled and rounded to a narrower integer range by (11) and (12), respectively. P_{DS} is the downscaled PSD value, R_{MAX} and R_{MIN} are the maximum and minimum values of the targeted range, respectively, whereas the P_{MAX} and P_{MIN} for the pre-scaled PSD values. R_{MAX} and R_{MIN} should be less than P_{MAX} and P_{MIN} , respectively. P_{DSR} is an FP PSD_{DS} value rounded off to an integer number.

$$P_{DS} = \left[(P - P_{MIN}) * \frac{R_{MAX} - R_{MIN}}{P_{MAX} - P_{MIN}} + R_{MIN} \right] \quad (11)$$

$$P_{DS} = \left[(P - P_{MIN}) * \frac{R_{MAXMINDIFF}}{P_{MAXMINDIFF}} + R_{MIN} \right] \quad (12)$$

R_{MAX} and R_{MIN} are 1 and 1024, respectively, for this work. P_{MAX} , P_{MIN} , R_{MAX} , and R_{MIN} are fixed FP parameters uploaded during the parameter uploading process. Therefore,

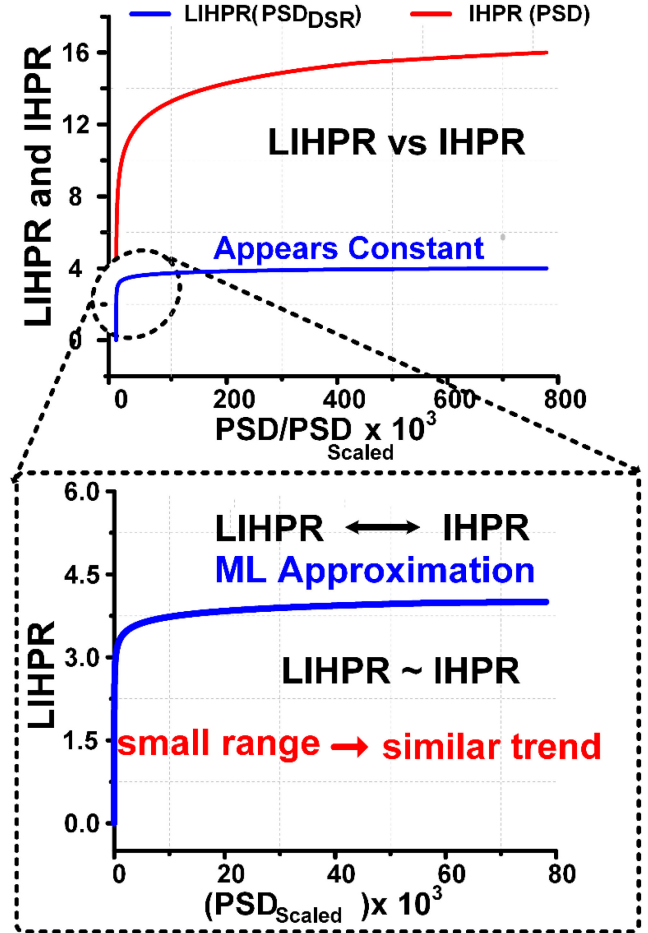


Fig. 13. LIHPR (PSD) and proposed LIHPR (PSD_{DSR}).

eq. (11) can be simplified as (12)–(14). SP_X and SP_Y in (14) are the scaling parameters for each channel. The scaling parameters SP_X and SP_Y for the selected channels are obtained from the parameter registers as SP.

$$P_{DS} = \left[\left(P * RP_{MAXMINDIFF} - P_{MIN} * RP_{MAXMINDIFF} \right) + R_{MIN} \right] \quad (13)$$

$$P_{DS} = [(P * SP_x) - SP_y] \quad (14)$$

$$P_{DSR} = \text{round}(P_{DS}) \quad (15)$$

LIHPR of PSD's in comparison to downscaled and rounded off PSD's is shown in Fig. 13. It shows that the LIHPR (PSD_{DSR}) has a much narrower and lower range than LIHPR (PSD) and seems a constant value when observed in comparison with IHPR. But the zoomed-in version has a similar trend in the narrower range (0–80).

The range and number of bits of PSD_{DSR} affect the classification accuracy and the hardware resources inversely. A narrower range/less number of bits (NoB's) for PSD_{DSR} degrades the ML classification accuracy, but enhances the area-efficiency, and vice-versa. Fig. 14 shows the trend that classification accuracy saturates for PSD_{DSR} NoB's of ≥ 10 . However, further reducing

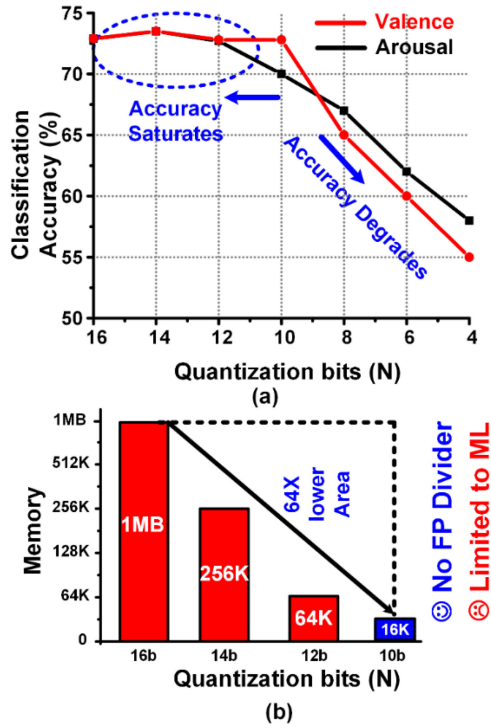


Fig. 14. Quantization effect on LIHPR for emotion's classification.

the NoB's for PSD_{DSR} degrades the classification accuracy by $\geq 5\%$.

The feature downscaling and rounding unit significantly reduced the memory resources for LUT based implementation of LIHPR to 64X. The proposed LDU replaces the division operation with 34% lesser area compared to piecewise linear and CORDIC algorithms for the division. But, the proposed implementation cannot be used for the general division and is customized for ML applications.

C. Feature Normalization Unit

The FNU in Fig. 11 calculates the normalized FV as defined in (10). The μ_{F1-16} and $1/\sigma_{F1-16}$ of the sixteen features are acquired from parameter register as N_1-N_{16} and $N_{17}-N_{32}$ respectively. Two 16×1 multiplexers are used to select the normalization parameters (N_A and N_B) of each feature using selection input NP-SEL. A 4b counter is used to generate NP-SEL. The normalized feature vector X_{NORM} is stored in a memory block (MEM-FV) of 16×16 b FP numbers as FN_1-FN_{16} and then forwarded to the CFU. FN_1-FN_{16} is forwarded to the CFU for valence and arousal classification.

D. Classification

The CFU calculates the labels of valence and arousal as positive (one) or negative (zero) using an LSVM classifier. The FN_{1-16} and pre-loaded classification parameters (VAL-P and ARR-P) for valence and arousal, respectively, are forwarded to the CFU by FE engine and parameter register, respectively. A 40 kHz clock (iCLK) is used to select the VAL-P or ARR-P

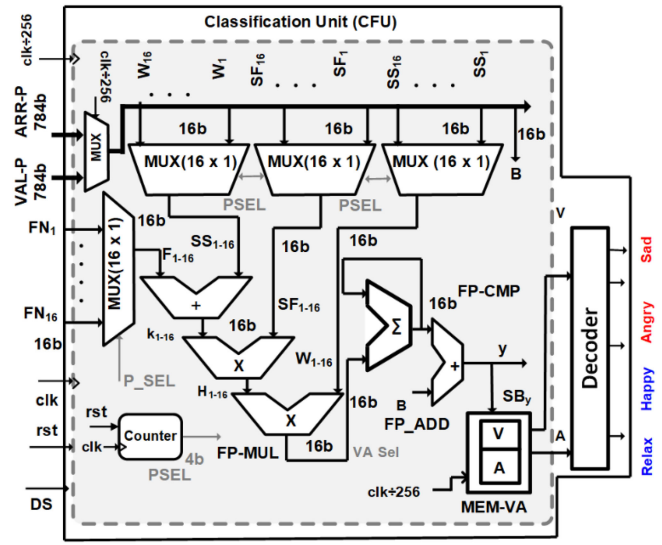


Fig. 15. Block-level implementation of CFU.

using a 2×1 multiplexer. An LSVM classifier is utilized to ensure area-and-power optimized hardware implementation.

$$k_{1-16} = [FN_{1-16} + SS_{1-16}] \quad (16)$$

$$H_{1-16} = [k_{1-16} * S F_{1-16}] \quad (17)$$

$$y = \sum_{k=1}^{16} W_k H_k + B \quad (18)$$

$$Valence/Arousal; = \begin{cases} 1, & y < 0 \\ 0, & y \geq 0 \end{cases} \quad (19)$$

LSVM performs a binary classification using weights (W), the scaled feature vector (H) and bias (B), defined in (16)–(19). H_{1-16} is obtained by adding the scale shift (SS_{1-16}) to the FN_{1-16} and then multiplying the intermediate vector named k_{1-16} with scale factor (SF_{1-16}) as in (16) and (17). The SS_{1-16} , SF_{1-16} , W_{1-16} , and B are extracted from the 784b VAL-P or ARR-P as shown in Fig. 15. Two 16b FP multipliers (FP-MUL), one 16b FP adder (FP-ADD), and one 16b FP accumulator (FP-ACCM) are used to implement (16)–(19). Three 16×1 multiplexers are used to select the SS_x , SF_x , W_x , and H_x from SS_{1-16} , SF_{1-16} , W_{1-16} , and H_{1-16} , respectively. The selection input (P-SEL) of the multiplexer is derived by a 4b counter as shown in Fig. 15.

The sign bit of y (SB_Y) is used for the valence/arousal classification. The SB_Y is stored in a memory block (MEM-VA) of 2×1 b for valence and arousal. Finally, emotion is determined based on the binary classification of the valence and arousal using a 2-to-4 decoder.

V. MEASUREMENT RESULTS AND PERFORMANCE

Fig. 16 shows the chip micrograph and the performance summary of the system. An 8-channel FE, 8-channel EEG-NAF classifier, and support vector (SV) cache is fabricated using a $0.18 \mu\text{m}$ 1P6M CMOS process with an active area of 5.4 mm^2 . EEG based emotion classification is performed using both PS

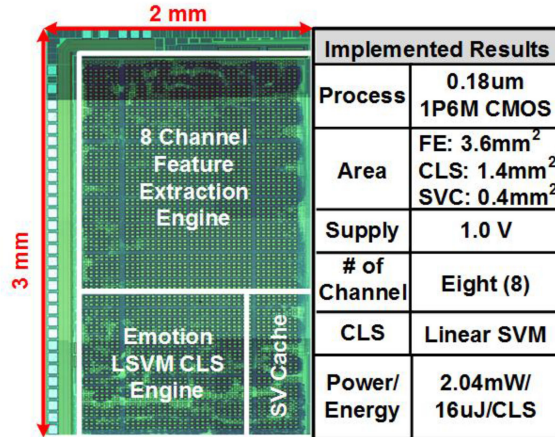


Fig. 16. Chip micrograph and performance summary of the system.

TABLE III
SUMMARY OF PATIENT-SPECIFIC/NON-PATIENT SPECIFIC
CLASSIFICATION RESULTS

Dataset	Patient-Specific		Non-patient-specific	
	Valence	Arousal	Valence	Arousal
DEAP	72.96 %	73.14 %	67.25 %	65.8 %
SEED	70.71 %	----	68.50 %	----

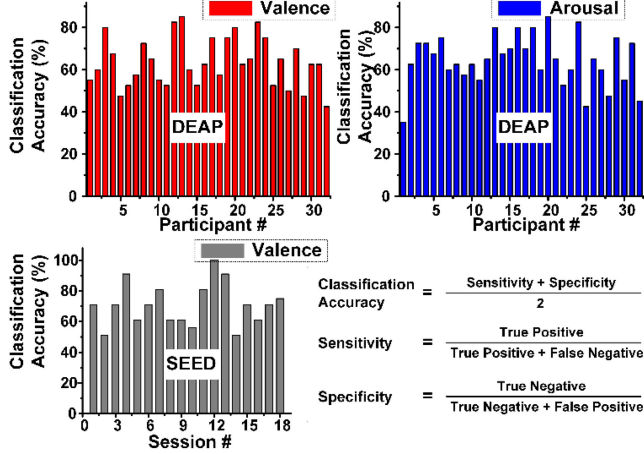


Fig. 17. Subject wise accuracies of valence and arousal on DEAP dataset and 18 different sessions on SEED dataset.

and NPS approach. The summary of the overall classification results using PS and NPS classification are shown in Table III.

The sensitivity and specificity of 73.0% and 73.1%, respectively, are achieved using the DEAP dataset, whereas, the sensitivity and specificity of 70.0% and 71.4%, respectively, are achieved using SEED. The subject-wise classification accuracies of all subjects in DEAP and 18 randomly chosen sessions in SEED are shown in Fig. 17. The subject wise statistics of each participant in DEAP containing gender, relative age, the number of positive and negative emotions are shown in Fig. 18.

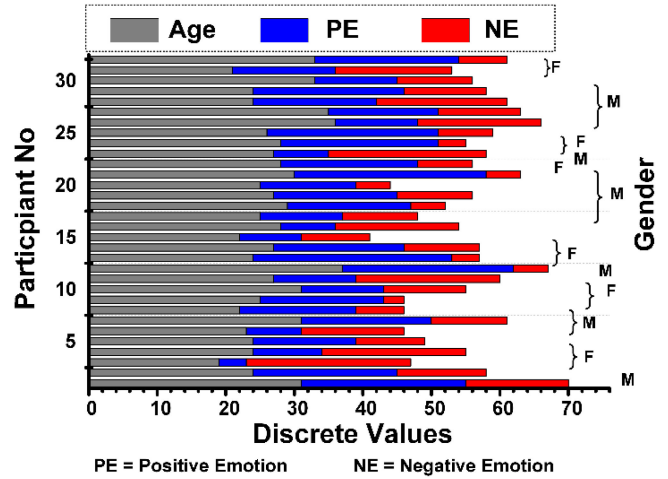


Fig. 18. Relative age count of positive and negative emotions and gender of each participant utilized in the analysis.

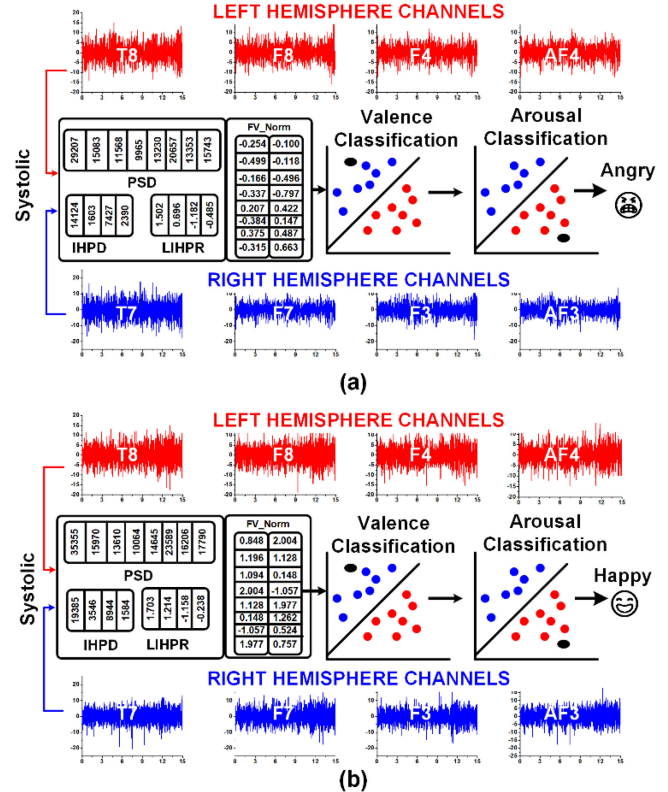


Fig. 19. LSVM emotion classification processor measurement results of (a) angry (b) happy emotion.

Classification accuracy was evaluated using the leave-one-out validation scheme because of its lower dependence on the data partitioned during training and testing split. The best-case accuracy reported for valence and arousal is $\sim 85\%$ and 82.5% , respectively, using DEAP and 100% for valence using SEED. Fig. 19 demonstrates the measurement result of two scenarios of angry and happy emotions. It shows the 15-sec of selected EEG channels for the trials (subject # 8) from the DEAP dataset that

TABLE IV
COMPARISON WITH THE STATE-OF-THE-ART WORKS

	S. Koelstra [21]	H. Ullah [29]	A. Aslam [33]	W. Fang [37]	W. Zheng [47]	M. Soleymani [62]	This Work
Hardware (Area/Power)	No -	No -	Yes (FPGA) (-/12.7mW)	Yes (28nm) (3.35mm ² /76.61mW)	No -	No -	Yes (0.18um- 1P6M) (5.4mm ² /2.04mW)
Dataset	DEAP	DEAP	DEAP	DEAP	DEAP, SEED	MAHNOB	DEAP, SEED
# of Channel	32	Variable	8	6	32,62	32	8
CLS	NB	SVM	SVM	CNN	GELM	LSTM RNN	SVM
Accuracy							
DEAP							
(VAL/ARR)	57.6/62.0	77.4/70.1	63/60	83.36/76.67	69.7/-	79.5/85.5	73.0/73.1
SEED (VAL)	-	-	-		91.1	-	70.7
Multiple BM-DS	No	No	No	No	Yes	No	Yes
Validation							

corresponds to these emotions. The valence and arousal values of 1.21 and 7.94 are classified as low valence (≤ 4) and high arousal (≥ 6), respectively, for the angry emotion.

Moreover, the valence and arousal values of 6.82 and 8.23 are classified as high valence (≥ 6) and high arousal (≥ 6) for happy emotion. The comparison with some state-of-the-art works is listed in Table III. Most of the previous works have not implemented the emotion detection system on hardware except [33], [37].

In [33] an FPGA based processor was designed with low classification accuracy and 7X more hardware resources compared to this work. Ref [62] has achieved a classification accuracy of 79.5% and 85.5% for valence and arousal, respectively. But have utilized a self-created dataset and relied on a higher number of EEG channels (32).

Ref [21] has reported a best-case accuracy of 57.6% for the valence and 62% for the arousal by using 16 EEG channels. Ref [47] has achieved an accuracy of 69.67% for valence using DEAP and 91.07% using SEED. However, they have used 32 EEG channels using DEAP and 64 channels using the SEED dataset. Ref [29] has achieved the classification accuracy of 77.4% and 70.1% using valence and arousal, respectively. However, they have used an automatic channel selection mechanism, which is not suitable for hardware implementation. Ref [37] is the only hardware implementation for a wearable emotion detection SoC. They have provided very good classification accuracies of 83.36% and 76.67% for valence and arousal, respectively, on the DEAP dataset using only six EEG channels. Their SoC implementation utilizes 28 nm CMOS technology using an area of 3.35 mm² and power consumption of 76.61 mW. Although their system has very good classification accuracy and

low area. But, an SoC based hardware implementation should be validated on multiple benchmark datasets, which they have not validated. The validation on multiple datasets ensures that the classification results are not biased or overfitted. The power consumption of their system is also 36X times higher than our system. This power consumption is high considering a wearable implementation.

In the implemented work, good classification accuracies of 72.96% and 73.14% are achieved on the DEAP [21] dataset for valence and arousal, respectively. The processor is also validated on the SEED [22] dataset with a classification accuracy of 70.71% for valence classification. This work utilizes eight EEG channels with minimum power (2.04 mW) consumption and classification energy (16 μ J/classification).

VI. CONCLUSION

In this paper, we have implemented the first SoC based 8-channel EEG patient-specific/non-specific emotion classification processor using LSVM classifier which can assist in the learning and cognitive development for CND patients. The proposed processor continuously detects human emotions using the valence and arousal classification. The processor is tested using DEAP and SEED emotion classification datasets.

The proposed system utilizes an area-and-energy efficient FE engine which is only based on PSD and reduces the overall area by 4.7X compared to the conventional implementations. Moreover, a LUT based log-2 divider is proposed which is 34% more area-efficient compared to the conventional divider. The PSED processor classifies valence and arousal with an accuracy of 72.96%, and 73.14%, respectively, for the DEAP

and valence with 70.71% for the SEED dataset. The proposed LSVM processor is fabricated using CMOS 180 nm process while consuming an overall power of 2.04 mW at 1 kHz with a system latency of 0.8 min for every classification.

ACKNOWLEDGMENT

The authors thank Cadence for its Academic CAD support and Muse Semiconductor for providing the tapeout services.

REFERENCES

- [1] H. Shi, H. Zhao, Y. Liu, W. Gao, and S. Dou, "Systematic analysis of a military wearable device based on a multi-level fusion framework: Research directions," *Sensors*, vol. 19, no. 12, pp. 2651–2672, Jun. 2019.
- [2] E. G-Velez, J. Feinstein, and D. Tranel, "Feelings without memory in alzheimer disease," *Cogn. Behav. Neurol.*, vol. 27, no. 3, pp. 117–129, Sep. 2014.
- [3] A. Kushki, A. Khan, J. Brian, and E. Anagnostou, "A kalman filtering framework for physiological detection of anxiety-related arousal in children with autism spectrum disorder," *IEEE Trans. Biomed. Eng. (TBME)*, vol. 62, no. 3, pp. 990–1000, Mar. 2015.
- [4] S. Leekam, "Social cognitive impairment and autism: What are we trying to explain?" *Philos. Trans. R. Soc. B*, vol. 371, no. 1686, pp. 1–8, Jan. 2016.
- [5] H. Ozhanl *et al.*, "Perception of Emotional Facial Expressions in Amyotrophic Lateral Sclerosis (ALS) at Behavioral and Brain Metabolic Level," *PLoS One*, vol. 11, no. 10, pp. 1–14, Oct. 2016.
- [6] A. Girardi, S. MacPherson, and S. Abrahams, "Deficits in emotional and social cognition in amyotrophic lateral sclerosis," *Neuropsychology*, vol. 25, no. 1, pp. 53–65, Jan. 2011.
- [7] E. M. Bouhabba, A. A. Shafie, and R. Akmeliawati, "Support vector machine for face emotion detection on real time basis," in *Proc. Int. Conf. Mechatronics (ICOM)*, May. 2011, pp. 1–6.
- [8] S. Turabzadeh, H. Meng, R. Swash, M. Pleva, and J. Juhar, "Real-time emotional state detection from facial expression on embedded devices," in *Proc. Int. Conf. Innovative Comput. Technol. (INTECH)*, Luton, 2017, pp. 46–51.
- [9] S. Porter and L. T. Brinke, "Reading between the lies: Identifying concealed and falsified emotions in universal facial expressions," *Psychol. Sci.*, vol. 19, no. 5, pp. 508–514, May 2008.
- [10] Q. Wu, B. Yan, Y. Zeng, C. Zhang, and L. Tong, "Anti-deception: Reliable EEG-based biometrics with real-time capability from the neural response of face rapid serial visual presentation," *Biomed. Eng. Online*, vol. 17, no. 1, pp. 1–13, Mar. 2018.
- [11] B. S. Mashford, A. Jimeno Yepes, I. Kiral-Kornek, J. Tang, and S. Harrer, "Neural-network-based analysis of EEG data using the neuromorphic TrueNorth chip for brain-machine interfaces," *IBM J. Res. Develop.*, vol. 61, no. 2–3, pp. 7:1–7:6, Mar.-May. 2017.
- [12] Z. Tayeb, E. Erçelik, and J. Conradt, "Decoding of motor imagery movements from EEG signals using SpiNNaker neuromorphic hardware," in *Proc. IEEE Eng. Med. Biol. Conf. Neural Eng. (NER)*, Aug. 2017, pp. 263–266.
- [13] S. Yang *et al.*, "Cost-efficient FPGA implementation of basal ganglia and their Parkinsonian analysis," *Neural Netw.*, vol. 71, pp. 62–75, Nov. 2015.
- [14] W. Saadeh, M. Altaf, and S. A. Butt, "A wearable neuro-degenerative diseases detection system based on gait dynamics," in *Proc. IFIP/IEEE Int. Conf. Very Large Scale Integr. (VLSI-SoC)*, Oct. 2017, pp. 1–6.
- [15] M. Bleichner *et al.*, "Exploring miniaturized EEG electrodes for brain-computer interfaces. An EEG you do not see?" *Physiol. Rep.*, pp. 1–9, Apr. 2015.
- [16] M. D. Gellman and J. R. Turner, *Encyclopedia of Behavioral Medicine*. New York, NY, USA: Springer, 2013, pp. 40–41.
- [17] P. Hill, D. Mroczek, and R. Young, "Personality traits as potential moderators of well-being," *Elsevier Stability Happiness*, pp. 245–259, 2014.
- [18] S. M. Alarcao and M. J. Fonseca, "Emotions recognition using eeg signals: A survey," *IEEE Trans. Affective Comput.*, vol. 10, no. 3, pp. 374–393, Jul. 2019.
- [19] S. Katsigiannis and N. Ramzan, "DREAMER: A database for emotion recognition through eeg and ecg signals from wireless low-cost off-the-shelf devices," *IEEE J. Biomed. Health Informat. (JBHI)*, vol. 22, no. 1, pp. 98–107, Jan. 2018.
- [20] P. Petrantonis and L. Hadjileontiadis, "Emotion recognition from eeg using higher order crossings," *IEEE Trans. Inf. Technol. Biomed.*, vol. 14, no. 2, pp. 186–197, Mar. 2010.
- [21] S. Koelstra *et al.*, "DEAP: A database for emotion analysis using physiological signals," *IEEE Trans. Affective Comput. (TAC)*, vol. 3, no. 1, pp. 18–31, Jan. 2012.
- [22] W. L. Zheng and B. Lu, "Investigating critical frequency bands and channels for eeg-based emotion recognition with deep neural networks," *IEEE Trans. Auton. Mental Dev.*, vol. 7, no. 3, pp. 162–175, Sep. 2015.
- [23] R. N. Duan *et al.*, "Differential entropy feature for EEG-based emotion classification," in *Proc. IEEE Eng. Med. Biol. Conf. Neural Eng. (NER)*, Sep. 2013, pp. 4202–4205.
- [24] X. Hu *et al.*, "EEG correlates of ten positive emotions," *Front. Human Neurosci.*, vol. 11, no. 1, pp. 1–26, Jan. 2017.
- [25] P. Lakhan *et al.*, "Consumer grade brain sensing for emotion recognition," *IEEE Sensors J.*, vol. 19, no. 21, pp. 9896–9907, 1 Nov. 2019.
- [26] Y. Lin, "Constructing a personalized cross-day eeg-based emotion-classification model using transfer learning," *IEEE J. Biomed. Health Informat. (JBHI)*, vol. 24, no. 5, pp. 1255–1264, May. 2020.
- [27] Y. Yang, Q. Wu, M. Qiu, Y. Wang, and X. Chen, "Emotion recognition from multi-channel eeg through parallel convolutional recurrent neural network," in *Proc. Int. Joint Conf. Neural Netw. (IJCNN)*, Jul. 2018, pp. 1–7.
- [28] T. Song, W. Zheng, C. Lu, Y. Zong, X. Zhang, and Z. Cui, "MPED: A multimodal physiological emotion database for discrete emotion recognition," *IEEE Access*, vol. 7, pp. 12177–12191, 2019.
- [29] H. Ullah, M. Uzair, A. Mahmood, M. Ullah, S. D. Khan, and F. A. Cheikh, "Internal emotion classification using eeg signal with sparse discriminative ensemble," *IEEE Access*, vol. 7, pp. 40144–40153, Mar. 2019.
- [30] M. Li, H. Xu, X. Liu, and S. Lu, "Emotion recognition from multichannel EEG signals using K-nearest neighbor classification," *Technol. Health Care*, vol. 26, no. S1, pp. 509–519, Apr. 2018.
- [31] H. Gonzalez, J. Yoo, and I. Elfadel, "EEG-based Emotion Detection Using Unsupervised Transfer Learning," in *Proc. IEEE Eng. Medicine Biol. Conf. (EMBC)*, Sep. 2019, pp. 694–697.
- [32] M. Taj-Eldin, C. Ryan, B. O'Flynn, and P. Galvin, "A Review of Wearable Solutions for Physiological and Emotional Monitoring for Use by People with Autism Spectrum Disorder and Their Caregivers," *Sensors*, vol. 18, no. 12, pp. 4271–4299, Dec. 2018.
- [33] A. Aslam and M. Altaf, "An 8 channel patient specific neuromorphic processor for the early screening of autistic children through emotion detection," in *Proc. IEEE Int. Symp. Circuits Syst. (ISCAS)*, May. 2019, pp. 1–5.
- [34] A. R. Aslam, T. Iqbal, M. Aftab, W. Saadeh, and M. Altaf, "A 10.13μJ/classification 2-channel Deep Neural Network-based SoC for Emotion Detection of Autistic Children," in *Proc. IEEE Custom Integr. Circuits Conf.*, Mar. 2020, pp. 1–4.
- [35] K. G. Smitha and A. P. Vinod, "Hardware efficient FPGA implementation of emotion recognizer for autistic children," in *Proc. IEEE Int. Conf. Electron. Comput. Commun. Technol.*, 2013, pp. 1–4.
- [36] R. Ramirez and Z. Vamvakousis, "Detecting emotion from EEG signals using the emotive epoch device," *Brain Informat. Lecture Notes Comput. Sci.*, vol. 7670, pp. 175–184, 2012.
- [37] W. Fang, K. Wang, N. Fahier, Y. Ho and Y. Huang, "Development and validation of an EEG-based real-time emotion recognition system using edge AI computing platform with convolutional neural network system-on-chip design," *IEEE J. Emerg. Sel. Topics Circuits Syst. (JETCAS)*, vol. 9, no. 4, pp. 645–657, Dec. 2019.
- [38] M. Altaf and J. Yoo, "A 1.83 μJ/classification, 8-channel, patient-specific epileptic seizure classification SoC using a non-linear support vector machine," *IEEE Trans. Biomed. Circuits Syst. (TBioCAS)*, vol. 10, no. 1, pp. 49–60, Feb. 2016.
- [39] Autism and Emotion Regulation, *Research Bulletin*, Center for Autism, no. 8, Feb. 2012.
- [40] The loneliness of Alexithymia. [Online]. Available: <https://www.mentalhelp.net/blogs/the-loneliness-of-alexithymia/>
- [41] S. B.-Cohen, O. Golani, and E. Ashwin, "Can emotion recognition be taught to children with autism spectrum conditions?," *Phil. Trans. R. Soc. B.*, vol. 364, no. 1535, pp. 3567–3574, Dec. 2009.
- [42] Y. Li, X. Zhang, B. Zhang, M. Lei, W. Cui, and Y. Guo, "A channel-projection mixed-scale convolutional neural network for motor imagery EEG decoding," *IEEE Trans. Neural Syst. Rehabil. Eng.*, vol. 27, no. 6, pp. 1170–1180, Jun. 2019.

- [43] W. Saadeh, F. Khan, and M. Altaf, "Design and implementation of a machine learning based EEG processor for accurate estimation of depth of anesthesia," *IEEE Trans. Biomed. Circuits Syst. (TBioCAS)*, vol. 13, no. 4, pp. 658–669, Aug. 2019.
- [44] R. Plutchik, "The nature of emotions," *Amer. Scientist*, pp. 60–179, July. 2003.
- [45] J. A. Russell, "A circumplex model of affect," *J. Personality Soc. Psychol.*, vol. 39, no. 6, pp. 1161–1178, Dec. 1980.
- [46] N. Oktavia, A. Wibawa, E. Pane, and M. Purnomo, "Human emotion classification based on EEG signals using Naïve bayes method," in *Proc. Int. Seminar Appl. for Technol. of Inf. Commun. (iSemantic)*, Sep. 2019, pp. 319–324.
- [47] W. Zheng, J. Zhu and B. Lu, "Identifying stable patterns over time for emotion recognition from EEG," *IEEE Trans. Affective Comput.*, vol. 10, no. 3, pp. 417–429, Jul. 2019.
- [48] W. Zheng, W. Liu, Y. Lu, B. Lu, and A. Cichocki, "EmotionMeter: A multimodal framework for recognizing human emotions," *IEEE Trans. Cybern.*, vol. 49, no. 3, pp. 1110–1122, Mar. 2019.
- [49] G. Titus and M. S. Sudhakar, "A simple but efficient EEG data compression algorithm for neuromorphic applications," *IETE J. Res.*, pp. 1–12, Jul. 2018.
- [50] M. Altaf and W. Saadeh, "A 0.21 μ J patient-specific REM/Non-REM sleep classifier for Alzheimer patients," in *Proc. IEEE Biomed. Circuits Syst. Conf. (BioCAS)*, Oct. 2017, pp. 652–655.
- [51] S. Zamin, M. A. B. Altaf, and W. Saadeh, "A Single Channel EEG-Based All Sleep Stages Classifier for Neurodegenerative Disorder," in *Proc. IEEE Biomed. Circuits Syst. (BioCAS)*, Oct. 2019, pp. 1–4.
- [52] P. A. Merolla, et al., "A million spiking-neuron integrated circuit with a scalable communication network and interface," *Science*, vol. 345, no. 6197, pp. 668–673, Aug. 2014.
- [53] S. Yang, et al., "Scalable digital neuromorphic architecture for large-scale biophysically meaningful neural network with multi-compartment neurons," *IEEE Trans. Neural Netw. Learning Syst.*, vol. 31, no. 1, pp. 148–162, Jan. 2020.
- [54] N. Jatupaiboon, S. Pan-Ngum, and P. Israsena, "Emotion classification using minimal EEG channels and frequency bands," in *Proc. 10th Int. Joint Conf. Comput. Sci. Softw. Eng.*, Aug. 2013, pp. 21–24.
- [55] F. Khan, U. Ashraf, M. Altaf, and W. Saadeh, "A patient-specific machine learning based EEG processor for accurate estimation of depth of anesthesia," in *Proc. IEEE Biomed. Circuits Syst. Conf. (BioCAS)*, Oct. 2018, pp. 507–510.
- [56] S. Sonnenburg and V. Franc, "COFFIN: A computational framework for linear SVMs," in *Proc. Int. Conf. Mach. Learn.*, Sep. 2010, pp. 999–1006.
- [57] I. Hmeidi, B. Hawashin, and E. Qawasmeh, "Performance of KNN and SVM classifiers on full word Arabic articles," *Advance Eng. Informat.*, no. 22, pp. 106–111, Dec. 2007.
- [58] M. A. B. Altaf, C. Zhang, and J. Yoo, "A 16-Channel patient-specific seizure onset and termination detection SoC with impedance-adaptive transcranial Electrical Stimulator," *IEEE J. Solid-State Circuits (JSSC)*, vol. 50, no. 11, pp. 2728–2740, Nov. 2015.
- [59] D. Lewis, "Complex logarithmic number system arithmetic using high-radix redundant CORDIC algorithms," in *Proc. IEEE Symp. Comput. Arithmetic*, Apr. 1999, pp. 194–203.
- [60] C. Liu, S. Ou, K. Chang, T. Lin, and S. Chen, "A low-error, cost-efficient design procedure for evaluating logarithms to Be used in a logarithmic arithmetic processor," *IEEE Trans. Comput.*, vol. 65, no. 4, pp. 1158–1164, 1 Apr. 2016.
- [61] D. Cantor, G. Estrin, and R. Turn, "Logarithmic and Exponential Function Evaluation in a Variable Structure Digital Computer," *IRE Trans. Electron. Comput.*, vol. EC-11, no. 2, pp. 155–164, April 1962.
- [62] M. Soleymani, S. A.-Esfeden, Y. Fu, and M. Pantic, "Analysis of EEG Signals and Facial Expressions for Continuous Emotion Detection," *IEEE Trans. Affective Comput. (TAC)*, vol. 7, no. 1, pp. 17–28, Jan. 2016.



Abdul Rehman Aslam (Student Member, IEEE) received the B.S. degree from the University of Engineering and Technology (UET), Taxila, Pakistan, in 2008, and the M.Sc. degree from the Lahore University of Management Sciences (LUMS), Lahore, Pakistan, in 2012, both in computer engineering. He is currently pursuing the PhD degree from LUMS in electrical engineering and working in the area of biomedical system on chip design. He was a faculty member in different universities in Pakistan from 2009 to 2014. In 2014, he joined UET Taxila as an Assistant Professor Computer Engineering. He is currently on study leave since 2017 from UET Taxila for his PhD studies at LUMS. His current research interest involves embedded systems, digital design, on-chip implementation of machine learning/deep learning algorithms and low power bio-medical processors with special focus on neurological disorders.



Muhammad Awais Bin Altaf (Member, IEEE) received the B.S. degree from the University of Engineering and Technology, Lahore, Pakistan, in 2008, and the M.Sc. and Ph.D. degrees in microsystems engineering and interdisciplinary engineering from the Masdar Institute of Science and Technology (MIST), Abu Dhabi, United Arab Emirates, in 2012 and 2016, respectively. From 2012 to 2013, he was a Digital Design Engineer Intern at Design Solutions, Global Foundries, Dresden, Germany, where he was involved in the implementation of digital test chips in support of 20 and 14 nm technologies. In 2015, he was an exchange-Ph.D. student with the Massachusetts Institute of Technology, Cambridge, MA, USA. During his stay at MIST, he developed an energy efficient machine-learning based feature extraction and classification processor for epileptic seizure detection. Since 2016, he has been with the Electrical Engineering Department, Lahore University of Management Sciences, Lahore, where he is currently an Assistant Professor. His current research interests include physiological signal monitoring, breast cancer detection, and the development of low-power mixed-signal circuits for the wearable and implantable medical applications.